Evaluation of Antioxidant, Anti-urease, Lipoxygenase, and Butyrylcholinesterase Inhibition Activities of Isatin Thiazole Derivatives Using Nano Formulations

[1]Khadim Mohi Uddin, [2]Najia Mansoor, [3]Syed Imran Ali, [4]Mohsin Ali*, [1]Mansoor Ahmed, [5]Mehwish Solangi, [1]Shazia Haider, and [5]Khalid Mohammed Khan

[1]*Department of Pharmaceutical Chemistry, University of Karachi, Karachi-75270, Pakistan.*
[2]*Department of Pharmacology, Faculty of Pharmacy, University of Karachi, Karachi-75270, Pakistan.*
[3]*Department of Applied Chemistry, University of Karachi, Karachi-75270, Pakistan.*
[4]*Department of Chemistry, University of Karachi, Karachi-75270, Pakistan.*
[5]*H. E. J. Research Institute of Chemistry, International Center for Chemical and Biological Sciences, University of Karachi, Karachi-75270, Pakistan*
mohsin.ali@uok.edu.pk*

(Received on 28th July 2025, accepted in revised form 5th December 2025)

Summary: This study investigates the enzyme inhibition and antioxidant activities of various nanoparticles loaded with three isatin thiazole derivatives. For drug encapsulation, two different nanoparticle systems were examined: polysaccharide-based nanoparticles, including alginate-chitosan nanoparticles (ACN) and gum-chitosan nanoparticles (GCN), and polymer-lipid hybrid nanoparticles based on the lipid soya lecithin in combination with either sodium alginate (PLHN-A) or gum acacia (PLHN-G). The biological activities of the drug-loaded nanoparticles were evaluated against key targets, including antioxidant activity, urease, lipoxygenase, and butyrylcholinesterase. The results were expressed as mean ± SEM, using eserine, butylated hydroxyanisole (BHA), and thiourea as reference standards. Among the tested systems, PLHN-A loaded with derivative-3 (D_3) exhibited the highest antioxidant activity (30.2 ± 0.45). Alginate-chitosan nanoparticles loaded with derivative-3 (ACN-D_3) demonstrated notable anti-urease activity (21.2 ± 0.12), while derivative-1(D_1) encapsulated in the same nanoparticle system (ACN-D_1) exhibited significant lipoxygenase inhibition (13.4 ± 0.48). Gum-chitosan nanoparticles loaded with derivative-1 (GCN-D_1) demonstrated strong butyrylcholinesterase inhibition (IC_{50} = 21.6 ± 0.17 µM). Overall, ACN and PLHN-A with all three derivatives (D_1, D_2 and D_3) emerged as promising candidates due to their excellent antioxidant and enzyme inhibition properties, underscoring the effect of nanoparticle composition on their biological activity and therapeutic potential.

Keywords: Nanoparticles, Antioxidant activity, Anti-urease activity, Lipoxygenase inhibition activity, Butyrylcholinesterase Inhibition Activity

Introduction

Enzyme inhibition is essential in biochemical and pharmacological research, providing critical insights into the development of therapeutic agents [1]. Oxidative stress, caused by an imbalance between reactive oxygen species (ROS) and antioxidant defenses, is implicated in many chronic diseases. Antioxidants that scavenge free radicals can mitigate ROS-induced damage and offer preventive benefits. Various natural compounds, including flavonoids and polyphenols, have demonstrated significant antioxidant activity [1, 2]. Among therapeutic enzyme targets, urease supports Helicobacter pylori survival by hydrolysing urea and raising gastric pH, contributing to gastrointestinal disorders [3, 4]. Thiazine Schiff bases and other compounds have shown urease inhibition in both in silico and in vitro studies [3-5]. Lipoxygenase, involved in leukotriene production, contributes to inflammation and is a target for the treatment of asthma and arthritis [6-9]. Similarly, butyrylcholinesterase, which is upregulated in Alzheimer's disease (AD), is linked to cognitive decline. Its inhibition can enhance acetylcholine levels and improve cognitive function [10, 11].

Promising enzyme inhibitors include benzoxazole and naphthoxazole derivatives with antioxidant and antiproliferative properties [12], dual-site pyrimidine and pyridine diamines and (α)-lipoic acid-based hybrids showing mixed inhibition of cholinesterases [13-15]. These findings support continued investigation of multifunctional compounds for the treatment of oxidative and enzyme-mediated disorders.

Isatin and its derivatives have been reported to exhibit a wide variety of biological activities, including antioxidant, anti-inflammatory, and enzyme inhibition properties [16-19]. Besides, many natural

*To whom all correspondence should be addressed.

and synthetic compounds containing a thiazole moiety exhibit potent biological activities and have been developed into valuable marketed drugs. Therefore, isatin and thiazole-based molecules are well recognized for their medicinal significance and biological activities [20-23]. In a recent study, Solangi et al. reported a new class of multifunctional compounds containing both isatin and thiazole functionalities [24]. These isatin thiazole derivatives exhibited moderate to good enzyme-inhibitory activities. However, despite these promising results, these compounds still suffer from some shortcomings. For instance, many isatin derivatives have poor water solubility and bioavailability, limiting their absorption and therapeutic efficacy. Additionally, isatin derivatives may degrade under physiological conditions, further reducing their effectiveness.

To address these limitations, encapsulation of drugs within biocompatible nanoparticles has emerged as a promising approach to improve the therapeutic efficacy and biological activity of pharmaceutical agents. Nanoparticle-based drug delivery systems have proven effective in enhancing drug stability, safety, and patient compliance for a wide range of drugs. Nanoparticles can improve drug stability within the body by preventing its direct contact with chemicals and enzymes. In addition to that, encapsulation can reduce drug toxicity by limiting its accumulation in healthy tissues. Nanoparticle based delivery systems provide sustained drug release thus maintaining consistent therapeutic levels in the body for prolong period of time, reducing dosing frequency and minimizing side effects [25, 26].

To mitigate the above mention limitations, in this study, we investigated the enzyme-inhibitory potential and antioxidant activity of three promising isatin thiazole derivatives (Figure-1) after their encapsulation in biodegradable nanoparticles. For the encapsulation, polysaccharide-based nanoparticles, namely alginate-chitosan nanoparticles (ACN) or gum acacia chitosan nanoparticles (GCN), were explored. Building on this approach, the study was extended to polymer-lipid hybrid nanoparticles (PLHN) comprised of lipid soya lecithin in combination with either sodium alginate (PLHN-A) or gum acacia (PLHN-G). The antioxidant potential and enzyme inhibition activity of these nanoparticles were systematically evaluated using established in vitro assays, including the DPPH radical scavenging assay for antioxidant activity and enzyme inhibition assays targeting urease, lipoxygenase, and butyrylcholinesterase. The results highlighted the therapeutic potential of isatin thiazole loaded nanoparticle systems as promising carriers for enzyme-targeted therapeutic applications. Altogether, the study presents a comprehensive analysis of the potential efficacy and therapeutic relevance of isatin thiazole derivatives and will be helpful for extending the applications of these compounds in treating oxidative stress-related and enzyme-mediated conditions [27-32].

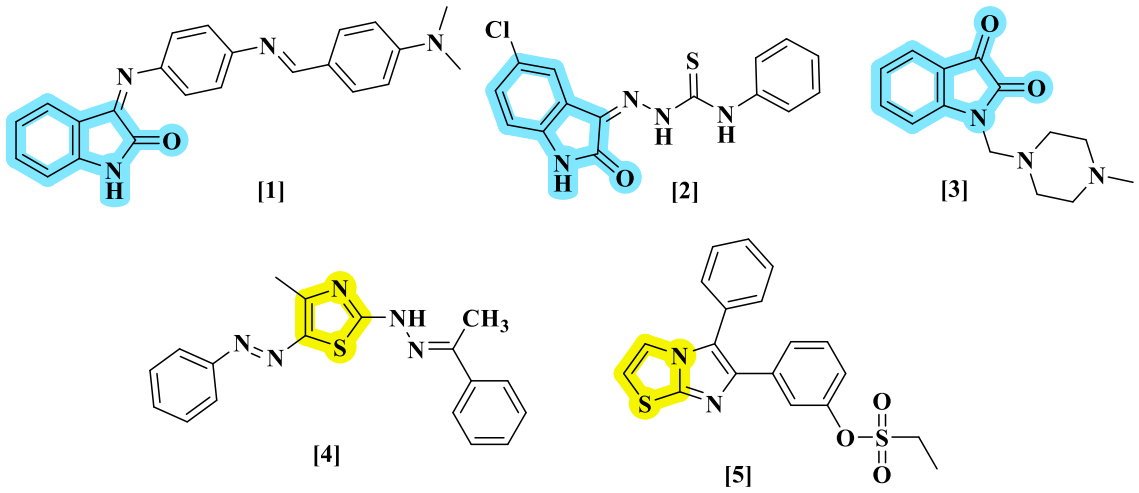

Fig. 1: Isatin and thiazole-based derivatives with biological activity.

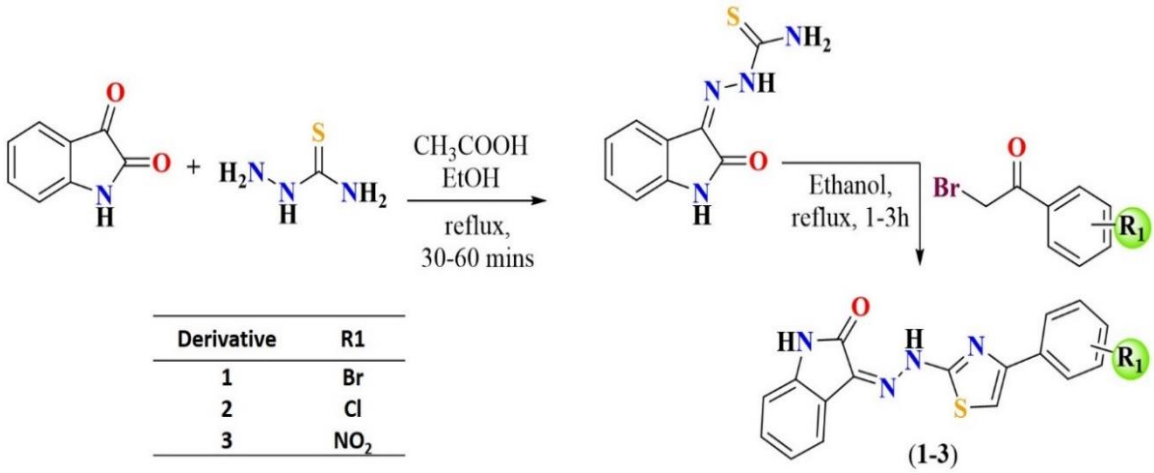

Derivative	R1
1	Br
2	Cl
3	NO_2

Scheme-1: Schematic representation for the synthesis of isatin-thiazole derivatives **1-3**.

Experimental

Materials and Methods

Chitosan (Mw: 190 - 375 kDa, >75% de-acetylated), sodium alginate (Mw: 12,000 - 40,000 Da and M:G ratio is 1.56,11.1 cps), and gum acacia (Mw: 180.41 g/mol) were purchased from Sigma Aldrich. The analytical-grade purity reagents including sodium hydroxide (NaOH, ≥98%), calcium chloride ($CaCl_2$, ≥97%), and acetic acid (CH_3COOH, glacial, ≥99.7%) were also purchased from Sigma Aldrich. Soya lecithin (≥95%) and tween-80 (≥99%) were provided by Martin Dow Ltd. Additionally, solvents such as chloroform (≥99%), ethanol (99.8%) and acetone (≥99.5%) were all purchased from Sigma Aldrich (USA) and used without further purification. Distilled and deionized water were routinely used in all experiments.

Three isatin thiazole derivatives; 3-(2-(4-(4-Bromophenyl)thiazol-2-yl)hydrazineylidene)indolin-2-one (**D_1**), 3-(2-(4-(4-Chlorophenyl)thiazol-2-yl)hydrazineylidene)indolin-2-one (**D_2**) and (3-(2-(4-(3-Nitrophenyl)thiazol-2-yl)hydrazineylidene)indolin-2-one (**D_3**) were all synthesized using the method reported by Solangi et al. [24]. The synthesis scheme is provided in Scheme-1. The enzymes used were Jack bean urease (Canavalia ensiformis), lipoxygenase, and butyrylcholinesterase were all purchased from Sigma Aldrich (USA).

Synthesis of drug encapsulated alginate-chitosan nanoparticle (ACN) and gum-chitosan nanoparticle (GCN)

The three isatin thiazole derivatives (D_1, D_2, and D_3; Scheme 1) were encapsulated in alginate-chitosan nanoparticles (ACN-D_1, ACN-D_2 and ACN-D_3) and gum-chitosan nanoparticles (GCN-D_1, GCN-D_2 and GCN-D_3) using the ionic gelation method. Briefly, a 10 mL solution of the isatin thiazole derivative (1 mg/mL, dissolved in acetone) was added dropwise to 110 mL solution (0.63%) of biopolymer (sodium alginate or gum acacia) under constant stirring. After 30 minutes, 7 mL of 36 mM $CaCl_2$ was added, followed by the dropwise addition of 25 mL of chitosan solution (0.63%, pH 4.9). Stirring was continued for 1 hour, and the dispersion was then incubated overnight. The nanoparticles were separated by centrifugation at 14,000 rpm, washed several times with water, dried, and stored in glass vials. Blank nanoparticles (ACN-Blank and GCN-Blank)) were also prepared using the same procedure without drug addition.

Synthesis of drug encapsulated polymer-lipid hybrid nanoparticles using sodium alginate (PLHN-A) and gum acacia (PLHN-G)

The three isatin thiazole derivatives were also encapsulated in Polymer-lipid hybrid nanoparticles using nanoprecipitation method. In all formulations, soya lecithin was used as lipid in combination with either the sodium alginate (PLHN-A) or gum acacia (PLHN- G). The notations PLHN-A-D_1, PLHN-A-D_2, and PLHN-A-D_3 represent the PLHN-A loaded with isatin thiazole derivatives D_1, D_2 and D_3 respectively. Similarly, PLHN- G-D_1, PLHN- G-D_2, and PLHN- G-D_3 represent the PLHN-G loaded with D_1, D_2 and D_3 respectively. The aqueous phase was prepared by dissolving 40 mg polymer (A or G) and 10 mg of Tween-80 (used as a surfactant) in 20 mL of deionized

water in a conical flask. Under continuous stirring, a drug solution (1 mg/mL, in acetone) was then added dropwise to this mixture. The organic phase was prepared by dissolving 40 mg soya lecithin in 10 mL of chloroform and subsequently, the resulting solution was added drop wise to the aqueous phase under continuous stirring for 60 minutes which resulted in a milky-white dispersion indicating the formation of nanoparticles. The resulting dispersion was left overnight to ensure uniform distribution of nanoparticles. The nanoparticles were then separated by centrifugation at 12,000 rpm, dried, and stored in glass vials. Blank nanoparticles (PLHN-A-Blank and PLHN-G-Blank) were also synthesized using the same method without loading of drug.

Characterization

The particle morphology was examined using scanning electron microscopy performed on a Quanta JEOL JSM-6390LV instrument. Before imaging, samples were prepared by applying a nanoparticle dispersion on a double-sided sticking tape attached on the surface of aluminum stub. Images were recorded using an operating voltage of 20 KV. The particle size distribution was performed using dynamic light scattering (DLS) performed at 25°C on a Malvern Zetasizer Nano ZS instrument. Each measurement was performed in triplicates. For sample centrifugation, a centrifuge 5804R was used, and sample preservation was done using freeze drying technique performed on a Trio Science TR-FD-BT-50 drier. Fourier transform infrared spectroscopy (FTIR) measurements were recorded on a Bruker Tensor 27 FT-IR instrument, in the range of 4000–400 cm-1using KBr discs.

Antioxidant Activity

The free radical scavenging activity of the samples was measured using the 1,1-diphenyl-2-picrylhydrazyl (DPPH) assay, following the method reported by Gulcin [33]. For the assay, 95µL aliquots of 0.3mM DPPH solution in ethanol were mixed with 5µL of each sample at various concentrations (62.5 µg/mL to 500µg/mL). After being spread out in a 96-well plate, the mixture plate was incubated for 30 minutes at 37°C. A microtiter plate reader (Spectramax Plus 384 Molecular Device, USA) was used to measure the absorbance at 515 nm. The percentage DPPH scavenging effect, taken as radical scavenging activity was calculated in relation to the control that was treated with methanol. The standard was butylated hydroxyanisole (BHA).

$$DPPH\ scavenging\ effect\ (\%) = \frac{Ac-As}{Ac} \times 100 \qquad (1)$$

Where, *Ac* is the absorbance of control (DMSO treated) and *As* represents the absorbance of samples.

Each experiment was performed three times, and data are presented as mean ± SEM from three independent experiments. SEM was calculated using the following formula.

$$SEM = \frac{SD}{\sqrt{n}} \qquad (2)$$

where SD is the standard deviation of the replicates and n = 3.

Anti-urease Activity

To measure the anti-urease activity, test compounds (5µL, 1mM) were incubated with reaction mixtures comprised of 25µL of jack bean urease enzymes (*Canavalia ensiformis*) solution and 55µL of buffers (comprising 0.01M $LiCl_2$, 1mM EDTA, and 0.01M $K_2HPO_4 \cdot 3H_2O$ with 100 mM urea) in 96-well plates for 15 minutes at 30°C. By measuring ammonia production using Weatherburn's indophenol method, urease activity was determined. In brief, each well received 70µL of alkali reagent (0.5% w/v NaOH and 0.1% active chloride NaOCl) and 45µL of phenol reagent (1% w/v phenol and 0.005% w/v sodium nitroprusside). A microplate reader (Molecular Device, USA) was used to measure the increasing absorbance at 630 nm after 50 minutes. Every reaction was carried out three times with a final volume of 200µL at pH 8.2. SoftMax Pro software was used to process the results. The percentage of urease inhibition was calculated using equation 3. Thiourea was used as the reference standard inhibitor [34]. Every experiment was conducted in triplicate, and the mean ± SEM was computed using the SEM equation 2.

$$Inhibition\ (\%) = 100 - \left(\frac{OD_{test\ well}}{OD_{control\ well}}\right) \times 100 \qquad (3)$$

Where, *OD test* is the absorbance of well containing the sample and *OD control* representing absorbance of the well without the inhibitor (only enzyme and substrate).

Lipoxygenase Inhibition Activity

Lipoxygenase (LOX) inhibition was measured by modified Tappel spectrophotometric method [35]. The reaction mixture contained 160 µL of sodium phosphate buffer (100 mM, pH 8.0), 10 µL of test solution, and 20 µL of LOX enzyme. After mixing the components, they were incubated at 25°C for 10 minutes. Subsequently,10 µL of the substrate solution (linoleic acid, 0.5 mM) and tween 20 (0.12%

w/v) in a 1:2 ratio was then added to start the reaction, and the change in absorbance at 234 nm was monitored for six minutes. In order to achieve a rate of 0.05 absorbance/min, the enzyme concentration in the reaction mixture was adjusted using a lipoxygenase enzyme solution. By observing the impact of increasing concentrations of these compounds in the assays on the degree of inhibition, the concentration of the test compound that inhibited lipoxygenase activity by 50% (IC_{50}) was found. The EZ-Fit Enzyme Kinetics Program (Perrella Scientific Inc., Amherst, USA) was used to calculate the IC_{50} values. All experiments were performed in triplicate, and results are expressed as mean ± SEM., calculated using equation 2.

Butyrylcholinesterase (BChE) Inhibition Activity

The butyrylcholinesterase (BChE) inhibition activity was performed according to Ellman method with few minor modifications [36]. The reaction mixture (100µL) contained 60µL of $Na_2H\ PO_4$ buffer, (50 mM, pH 7.7), 10µL of BChE (0.5-units/well) was added after 10µL of the test compound (0.5 mM/well) (Sigma Inc.). The contents were mixed, pre-read at 405 nm, and then pre-incubated for 10 minutes at 37°C. To initiate the reaction, 10µL of butyryl thiocholine chloride (0.5 mM/well) substrate was added. Following that 10µL of and (5,5'-dithiobis-(2-nitrobenzoic acid) (DTNB, 0.5 mM/well) was added. After 15 minutes of incubation at 37°C, absorbance was measured at 405 nm using a 96-well plate reader (Synergy HT, Biotek, USA). Each experiment had a corresponding control and was conducted in triplicate. They used standard eserine (0.5 mM/well). IC_{50} values were computed using the EZ-Fit Enzyme Kinetics software (Perrella Scientific Inc., Amherst, USA). Each experiment was conducted in triplicate and the results are presented as mean ± SEM computed using equation 2.

Results and Discussion

Characterization of Nanoparticles

The particle size distribution of the nanoparticle is presented in Figure 2A. This figure provides a comprehensive characterization of the nanoparticles synthesized via the ionic gelation method, particularly focusing on their size profiles. GCN-D_1 displayed a mean particle size of approximately 220 nm, with the size distribution of GCN-D_1 loaded GCN exhibiting a peak centered on this value. Dynamic Light Scattering (DLS) analysis confirms that the formulation maintains a uniform particle size distribution with minimal polydispersity.

Scanning Electron Microscopy (SEM) images of the nanoparticles, also shown in Figure 2B, reveal the surface morphology of the isatin-thiazole derivative-loaded particles. For GCN-D_1, the SEM micrographs indicate a relatively monodispersed population of spherical nanoparticles, which correlates well with the DLS findings. In addition to well-dispersed particles, a few larger aggregates are also observed likely formed during the sample preparation process for SEM imaging.

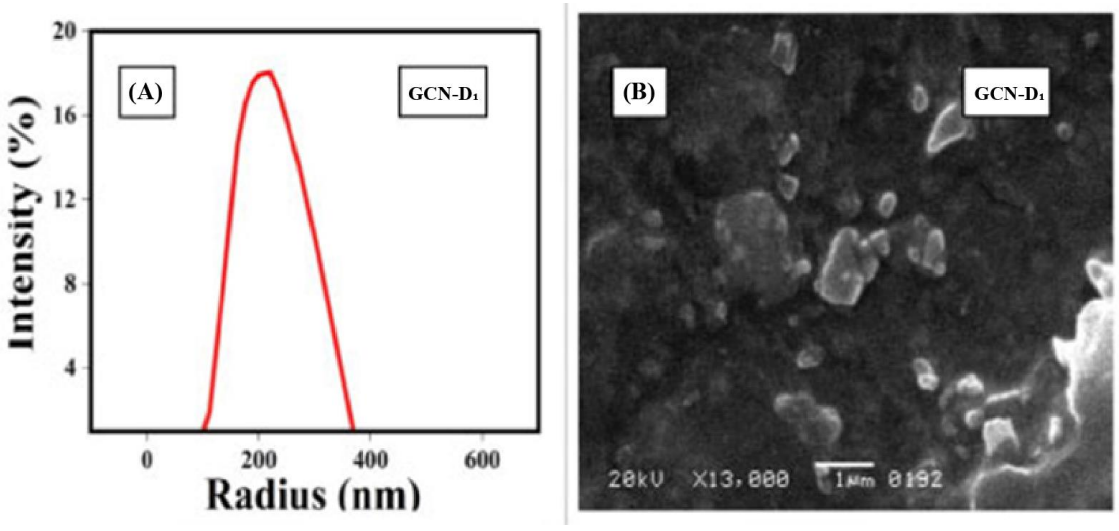

Fig. 2: Particle size distribution and SEM micrograph of isatin thiazole derivative (D_1, scheme 1) encapsulated in gum-chitosan nanoparticles (GCN-D_1) prepared by ionic gelation method.

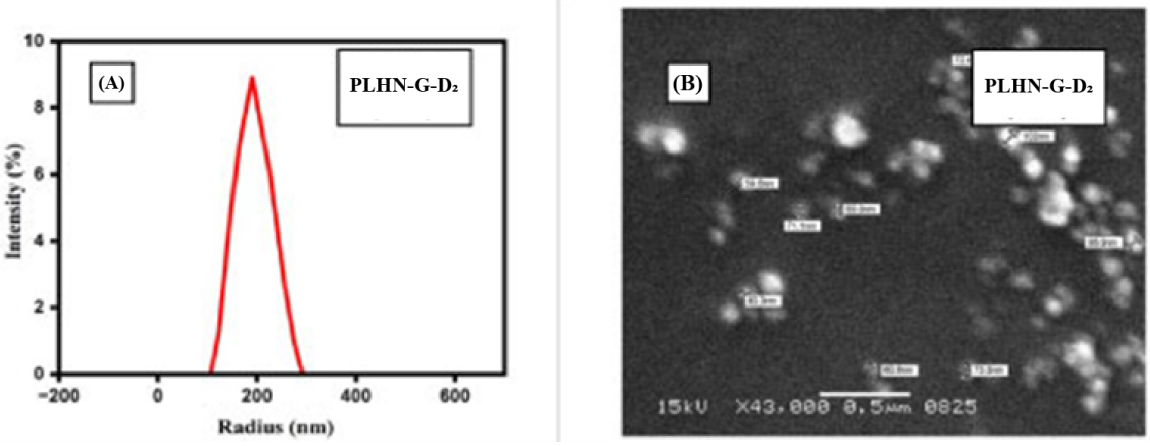

Fig. 3: Particle size distribution and SEM micrograph of isatin thiazole derivative (D_2, scheme 1) encapsulated in Polymer-lipid hybrid nanoparticles with gum (PLHN-G-D_2) prepared by nanoprecipitation method.

Similarly, dynamic light scattering (DLS) analysis was performed to determine the particle size distribution of drug-loaded nanoparticles. As shown in Figure 3A, nanoparticles were formulated using the nanoprecipitation method. Among them, polymer-lipid hybrid nanoparticles with gum acacia (PLHN-G), PLHN-G-D_2, exhibited the smallest particle size, measuring approximately 190 nm. The particle size distribution curve showed a sharp peak centered at 190 nm, indicating a narrow and uniform size distribution with minimal variation, suggesting high formulation stability.

Scanning electron microscopy (SEM) images of isatin thiazole derivative-loaded nanoparticles are presented in Figure 3B. The SEM micrographs of the PLHN-G-D_2 revealed a relatively monodispersed population of spherical nanoparticles, which correlated well with DLS data. Additionally, some larger aggregates were observed, likely resulting from sample drying or handling during SEM sample preparation, rather than a feature of the formulation itself.

FTIR Characterization

In Figure-4a shows the overlay spectra obtained from FTIR analysis of polymers sodium alginate, chitosan and gum acacia. The similarities in the spectra of polymer are due to the presence of common functional groups characteristic of polysaccharides. All three polymers have hydroxyl (-OH) groups, which exhibit a broad absorption band around 3200-3550 cm^{-1} due to the O-H stretching vibrations. Furthermore, C-H stretching vibrations in the region around 2850-2975 cm^{-1} are also visible Sodium alginate in particular, displayed O-H stretch at 3132 cm^{-1}, C-H bending around 1400 cm^{-1}, and C-O stretching vibrations appearing as doublets at 1090 cm^{-1} and 1030 cm^{-1}. Gum acacia also has carboxyl groups in the uronic acids moieties, which is seen in the form of characteristic absorptions peaks in the carbonyl region. Chitosan displayed absorption bands due to amide group (C=O stretching), around 1640-1650 cm-1, as well as amino groups (NH_2), which exhibited characteristic bands around 1550-1650 cm^{-1} (N-H bending) and 3200-3500 cm^{-1} (N-H stretching). The FTIR spectrum of soya lecithin showed aliphatic carbon (C-H) bending at 1400 cm^{-1}, a strong C=C stretch at 1647 cm^{-1}, and a C-H alkene stretching peak at 3119 cm^{-1}.

In Figure 4b, the FTIR spectra of the three derivatives is presented. Along with the several common features, some distinct peaks arising from their unique substituents are also visible. All the three derivative displayed N-H stretching vibrations around 3200-3500 cm^{-1}, strong C=O stretching peaks between 1650-1750 cm^{-1}, and C=N stretching vibrations around 1500-1600 cm^{-1}. Additionally, aromatic C=C stretching bands were observed in 1400-1600 cm^{-1} range, while C-H stretching vibrations were observed around 2850-2950 cm^{-1}. Peaks due to C-S stretching vibrations in the thiazole rings appeared in the 600-800 cm^{-1} range. Moreover, each derivative showed certain distinct peaks, reflecting its specific substituent. For D_1, with 4-bromo substitution, evident C-Br stretching peaks were observed in the range of 500-600 cm^{-1}. The spectra of D_2, with 4-chloro substitution, showed C-Cl stretching peaks around 700-800 cm^{-1}. In the spectra of derivative D_3, with 3-nitro group, a distinctive NO_2 stretching peaks, with asymmetric stretching around 1500-1600 cm^{-1} and

symmetric stretching between 1300-1400 cm^{-1} were observed.

In Figure 4c, the spectra represent gum acacia-chitosan nanoparticles (GCN) encapsulated with D_1 is presented. The spectra of GCN-D_1, showed reduced band intensity in the 4000–3000 cm^{-1} region compared with the both polymers, gum acacia and chitosan, while exhibiting higher intensity relative to the pure derivative. Furthermore, GCN-D_1 retained the characteristic functional group peaks of the isatin-thiazole derivative within their respective ranges, indicating successful encapsulation and incorporation of derivative into the synthesized gum acacia-chitosan nanoparticles.

In Figure 4c, the FTIR spectra of polymer-lipid hybrid nanoparticles containing gum acacia (PLHN-G) encapsulated with D_2 is presented. The synthesized PLHN-G-D_2 displayed reduced intensity in the peaks around the 4000-3000 cm^{-1} range compared to gum acacia. However, an increase in peak intensity within same region was observed for PLHN-G-D_2 relative to the pure D_2. In addition, PLHN-G-D_2 demonstrated characteristic functional group peaks of the D_2 within their indicated range. These characteristic peaks confirm the successful encapsulation and complete incorporation of the D_2 into the synthesized PLHN-G-D_2.

Biological Activity Evaluation

A comprehensive overview of various enzyme-inhibition activities and the antioxidant potential of several compounds is listed in Table 1. The table includes data on antioxidant activity, anti-urease activity, lipoxygenase inhibition, and butyrylcholinesterase inhibition. Each activity is expressed as mean ± standard error of the mean (SEM), while butyrylcholinesterase inhibition is reported as IC_{50} values (µM). Butyrylcholinesterase inhibition activity is measured as IC_{50}, the concentration required to inhibit 50% of the enzyme activity. GCN-D_2 had the lowest IC_{50} value (22.2 ± 0.06 µM), indicating potent inhibition of butyrylcholinesterase, which is relevant for neurodegenerative disease treatment.

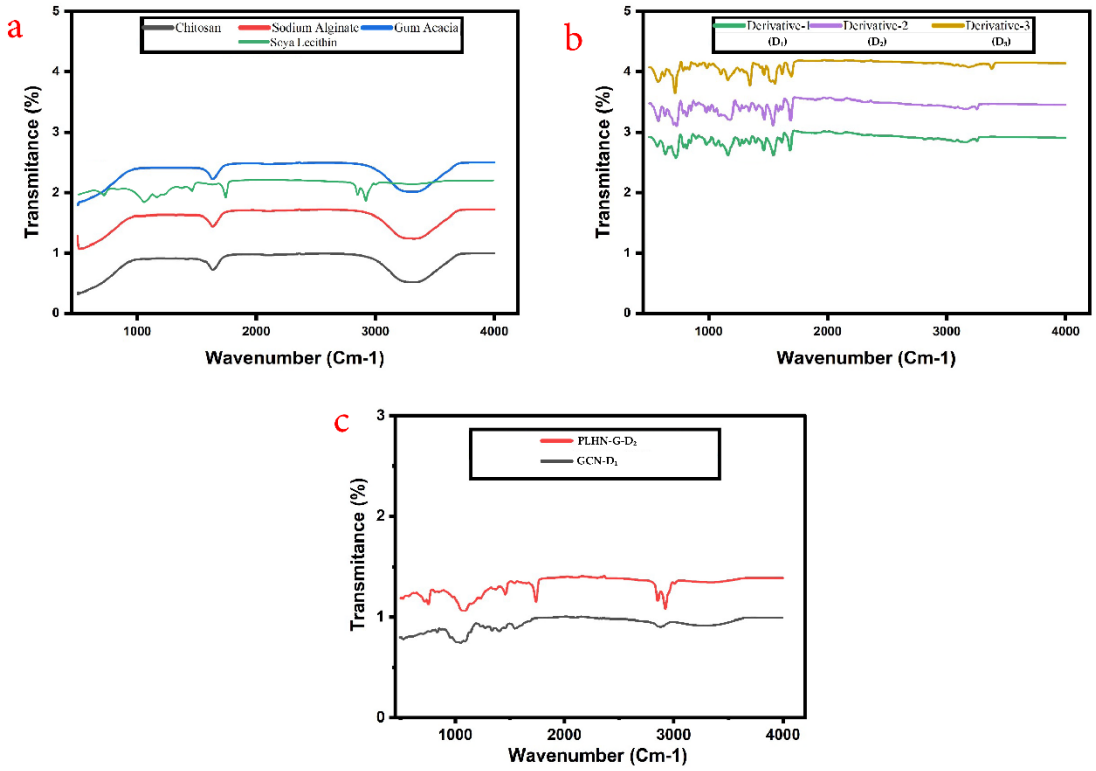

Fig. 4: (a) FTIR overlay of polymer and soya lecithin. (b) FTIR overlay of isatin thiazole derivatives (D_1, D_2 and D_3). (c) FTIR overlay of gum acacia-chitosan nanoparticle (GCN) with D_1 and polymer-lipid hybrid nanoparticles contain gum acacia (PLHN-G) with D_2.

Table-1: Enzyme Activities of Various Compounds.

Comp. No.	Antioxidant Activity (Mean ± SEM) n=3	Anti-urease Activity (Mean ± SEM) n=3	Lipoxygenase Inhibition Activity (Mean ± SEM) n=3	Butyrylcholinesterase Inhibition Activity IC_{50} (µM) n=3
ACN-D_1	34.2 ± 0.42	29.4 ± 0.11	13.4 ± 0.48	32.4 ± 0.21
ACN-D_2	41.5 ± 0.15	32.1 ± 0.99	22.1 ± 0.28	63.5 ± 0.95
ACN-D_3	52.2 ± 0.23	21.2 ± 0.12	29.3 ± 0.4	78.6 ± 0.46
GCN-D_1	82.9 ± 0.39	82.1 ± 0.28	39.2 ± 0.12	21.6 ± 0.17
GCN-D_2	76.5 ± 0.49	77.7 ± 0.11	49.7 ± 0.72	22.2 ± 0.06
GCN-D_3	71.1 ± 0.28	62.4 ± 0.09	52.3 ± 0.17	31.9 ± 0.48
PLHN-A-D_1	33.3 ± 0.28	29.5 ± 0.41	27.1 ± 0.29	76.8 ± 0.37
PLHN-A-D_2	39.5 ± 0.14	27.3 ± 0.21	39.2 ± 0.14	87.6 ± 0.63
PLHN-A-D_3	30.2 ± 0.45	42.4 ± 0.10	14.5 ± 0.78	65.9 ± 0.19
PLHN-G-D_1	51.4 ± 0.29	36.4 ± 0.24	85.2 ± 0.11	78.8 ± 0.65
PLHN-G-D_2	59.5 ± 0.45	89.2 ± 0.34	89.1 ± 0.27	80.9 ± 0.28
PLHN-G-D_3	62.3 ± 0.23	58.4 ± 0.12	76.4 ± 0.69	45.6 ± 0.71
Eserine				7.8 ± 0.28
BHA	44.2 ± 0.46		22.4 ± 0.41	
Thiourea		21.5 ± 0.47		
Derivative-1 (D_1)	20.61 ± 0.11	21.38 ± 0.11	40.65 ± 0.02	27.02 ± 0.11
Derivative-2 (D_2)	17.01 ± 0.12	18.67 ± 0.03	15.70 ± 0.08	26.46 ± 0.06
Derivative-3 (D_3)	21.77 ± 0.07	27.33 ± 0.15	32.16 ± 0.06	27.12 ± 0.17

Antioxidant Activity

The antioxidant activity of various compounds was assessed and compared with the standard antioxidant BHA (butylated hydroxyanisole), and the results were summarized as mean ± SEM. The data highlights significant differences in the antioxidant capabilities of the tested compounds. The alginate chitosan nanoparticles (ACN) showed a progressive increase in antioxidant activity from ACN-D_1 to ACN-D_3, indicating that radical stabilisation and electron donation are influenced by substitution on the thiazole ring [37]. ACN-D_1 and ACN-D_2 both exhibited excellent antioxidant activity within these nanoparticles as compared to the standard BHA (44.2±0.46). It suggests that ACN-D_1 and ACN-D_2 could be more effective antioxidants than BHA, while ACN-D_3 has moderate antioxidant capabilities. The gum-chitosan nanoparticles (GCN) demonstrated lower antioxidant activities compared to the standard BHA. GCN-D_1 has very low antioxidant activity (82.9±0.39), followed by GCN-D_2 (76.5±0.49) and GCN-D_3 (71.1±0.28). Probably because of its lower molecular weight and insufficient cross-linking, leading to reduced interaction with biological targets and faster drug leakage [38].

The antioxidant activity of the polymer-lipid hybrid nanoparticles containing sodium alginate (PLHN-A) increased gradually from PLHN-A-D_1 to PLHN-A-D_3. The nanoparticles containing PLHN-A-D_1, PLHN-A-D_2 and PLHN-A-D_3 exhibited superior antioxidant activity when compared to the standard BHA (44.2±0.46). It indicates that PLHN-A-D_1, PLHN-A-D_2 and PLHN-A-D_3 may function as antioxidants more potent than BHA. This improved performance is likely due to the synergistic interaction between sodium alginate and soya lecithin, which enhanced the active compound's dispersion and controlled release, making it more accessible to free radicals [39]. Comparing the polymer-lipid hybrid nanoparticles with gum acacia (PLHN-G) to the standard BHA, the value demonstrated weaker antioxidant activity. PLHN-G-D_3 has very low antioxidant activity (62.3 ± 0.23), followed by PLHN-G-D_2 (59.5 ± 0.45) and PLHN-G-D_1 (51.4 ± 0.29) showed better activity as compared to the other one. Weaker electrostatic interaction between gum acacia and the lipid phase and less effective drug encapsulation could be the cause of the decreased activity [40].

Anti-Urease Activity

The anti-urease activity of nanoparticles was evaluated, and the results were expressed as mean ± SEM. The standard used for comparison was thiourea, with an anti-urease activity of 21.5 ± 0.47. The data reveals notable differences in the anti-urease capabilities of the nanoparticles.

The alginate chitosan nanoparticles showed varying levels of anti-urease activity with ACN-D_2 exhibited the moderate activity in this series (32.1 ± 0.99). ACN-D_3 (21.2 ± 0.12) had activity comparable to that of the standard Thiourea (21.5 ± 0.47). This may likely result from the smaller particle size and negative surface charge, facilitating better enzyme access [41]. ACN-D_1 also demonstrated moderate activity (29.4 ± 0.11), lower than the standard but higher than ACN-D_2. The gum-chitosan nanoparticles (GCN) showed lower anti-urease activity compared to the standard Thiourea. GCN-D_1 had the lowest activity (82.1 ± 0.28), followed closely by GCN-D_2 (77.7 ± 0.11) and GCN-D_3 (62.4 ± 0.09). These results suggest that the GCN are very weaker anti-urease agents than the standard Thiourea, confirming that gum acacia provided less favorable conditions for drug enzyme interaction [42].

The anti-urease activity of the polymer-lipid hybrid nanoparticles containing sodium alginate (PLHN-A) showed good activity for all the encapsulated drugs (D_1, D_2, and D_3). The nanoparticles containing the three derivatives, PLHN-A-D_1 PLHN-A-D_2 and PLHN-A-D_3 exhibited good activity when compared to the standard Thiourea (21.5 ± 0.47). Comparing the polymer-lipid hybrid nanoparticles with gum acacia (PLHN-G) to the standard Thiourea (21.5 ± 0.47), the value demonstrated weaker antiurease activity. PLHN-G-D_2 has very low antiurease activity (89.2 ± 0.34) followed by PLHN-G-D_3 (58.4 ± 0.12) and PLHN-G-D_1 (36.4 ± 0.24) showed very less activity as compared to standard. This is likely due to the slower drug release, which restricts the active molecule's instant access to the enzyme [43].

Lipoxygenase (LOX) Inhibition

The evaluation of the lipoxygenase inhibition activity of nanoparticles was conducted, and the mean ± SEM results were reported. BHA (butylated hydroxyanisole) was the benchmark utilized for comparison, possessing a lipoxygenase inhibition activity of 22.4 ± 0.41.

The alginate chitosan nanoparticles (ACN) showed a range of lipoxygenase inhibition activities. ACN-D_1 had the highest activity (13.4 ± 0.48), which was compared to the standard BHA and indicating stronger inhibition of lipoxygenase compared to BHA. This may be due to the result of its enhanced diffusion across the enzyme interface and high surface charge [44]. ACN-D_2 (22.1 ± 0.28) showed similarly activity comparable to BHA (22.4 ± 0.41). ACN-D_3 also showed good activity (29.3 ± 0.4). The lipoxygenase inhibition activities of the Gum-chitosan nanoparticles (GCN) were found to be lower than those of standard BHA (22.4 ± 0.41). GCN-D_1 (39.2 ± 0.12) exhibited good activity, while GCN-D_3 (52.3 ± 0.17) and GCN-D_2 (49.7 ± 0.72) were in close succession. According to these findings, GCN are relatively mild lipoxygenase agents in comparison to regular BHA.

The lipoxygenase inhibition activity of the polymer-lipid hybrid nanoparticles containing sodium alginate (PLHN-A) showed good activity from PLHN-A-D_1 to PLHN-A-D_3. The PLHN-A-D_3 (14.5 ± 0.78) showed excellent activity which supports that the alginate-lecithin interface promotes optimal drug orientation for enzyme binding [45]. PLHN-A-D_1 (27.1 ± 0.29) and PLHN-A-D_2 (39.2 ± 0.14) had good and moderate activity compared to the standard BHA (22.4 ± 0.41). The lipoxygenase inhibition activity of the polymer-lipid hybrid nanoparticles containing gum acacia (PLHN-G) showed very weak activity from PLHN-G-D_1 to PLHN-G-D_3. PLHN-G-D_2 has very low lipoxygenase inhibition activity (89.2 ± 0.34) followed by PLHN-G-D_1 (85.2 ± 0.11) and PLHN-G-D_3 (76.4 ± 0.69) showed very low activity compared to standard BHA (22.4 ± 0.41) which is likely due to its larger particle size and restricted lipoxygenase active site interaction [46].

Butyrylcholinesterase (BChE) Inhibition

The butyrylcholinesterase (BChE) inhibition activity of various compounds was evaluated, with results expressed as IC_{50} values (μM) ± SEM. The standard used for comparison was Eserine, with an IC_{50} of 7.8 ± 0.28 μM.

The alginate chitosan nanoparticles (ACN) showed moderate to low BChE inhibition activities. ACN-D_1 exhibited the lowest IC_{50} value (32.4 ± 0.21 μM), indicating better inhibition compared to ACN-D_2 and ACN-D_3, but still significantly less potent than the standard Eserine. ACN-D_2 and ACN-D_3 had higher IC_{50} values (63.5 ± 0.95μM and 78.6 ± 0.46μM, respectively), indicating weaker inhibition. The gum chitosan nanoparticles (GCN) exhibited lower IC_{50} values, indicating stronger BChE inhibition compared to the (ACN). GCN-D_1 had the lowest IC_{50} (21.6 ± 0.17 μM), followed closely by GCN-D_2 (22.2 ± 0.06 μM), both of which demonstrated significant inhibition but were still less potent than Eserine (7.8 ± 0.28 μM). GCN-D_3 showed a slightly higher IC_{50} (31.9 ± 0.48 μM) but was still more effective than most of the (ACN), suggesting that gum-based carriers may enhance interaction with cholinesterase active sites [47].

The polymer-lipid hybrid nanoparticles containing sodium alginate (PLHN-A) showed higher IC_{50} values, indicating weaker BChE inhibition. Among them, PLHN-A-D_3 had the lowest IC_{50} (65.9 ± 0.19 μM), followed by PLHN-A-D_1 (76.8 ± 0.37 μM) and PLHN-A-D_2 (87.6 ± 0.63 μM). These values suggest moderate to low inhibition activity compared to eserine (7.8 ± 0.28 μM). The polymer-lipid hybrid nanoparticles containing gum (PLHN-G) exhibited varying levels of inhibition activities. PLHN-G-D_3 had the lowest IC_{50} (45.6 ± 0.71 μM), indicating better inhibition compared to PLHN-G-D_1 and PLHN-G-D_2 but still less potent than Eserine (7.8 ± 0.28 μM). PLHN-G-D_1 and PLHN-G-D_2 showed higher IC_{50} values (78.8 ± 0.65 μM and 80.9 ± 0.28 μM, respectively), indicating weaker inhibition. Slower drug release from the sodium alginate-lecithin matrix may be the cause of the decreased potency observed in PLHN-A, indicating regulated but restricted immediate enzyme accessibility [48].

Table-2: Comparative Analysis of Enzyme Inhibition Activities.

Activity Type	Standard Activity	Highest Activity	Lowest Activity
Antioxidant	**BHA (44.2±0.46)**	**PLHN-A-D_3 (30.2±0.45)**	**GCN-D_1 (82.9±0.39)**
Anti-urease	**Thiourea (21.5 ± 0.47)**	**ACN-D_3 (21.2 ± 0.12)**	**PLHN-G-D_2 (89.2 ± 0.34)**
Lipoxygenase	**BHA (22.4±0.41)**	**ACN-D_1 (13.4 ± 0.48)**	**PLHN-G-D_2 (89.1 ±0.27)**
Butyrylcholinesterase	**Eserine (7.8 ± 0.28)**	**GCN-D_1 (21.6 ± 0.17)**	**PLHN-A-D_2 (87.6 ± 0.63)**

Table-2 provides a comparative analysis of enzyme inhibition activities among the tested compounds. For antioxidant activity, PLHN-A-D_3 demonstrated the highest effectiveness with an impressive (30.2±0.45), because sodium alginate and soya lecithin worked in combination to improve the dispersion and controlled release of the active compound, increasing its accessibility to free radicals [39]. While GCN-D_1 exhibited the lowest activity at (82.9±0.39), likely due to reduced molecular weight and ineffective cross-linking, which causes less surface interaction with biological targets and quicker drug leakage [38]. In terms of anti-urease activity, ACN-D_3 showed the highest inhibition with (21.2 ± 0.12), because smaller particle size and negative surface charge, facilitating better enzyme access [40]. While PLHN-G-D_2, had the lowest inhibition at (89.2 ± 0.34), likely due to slower drug release, which limits the active molecule's immediate access to the enzyme [42]. For lipoxygenase inhibition, ACN-D_1 led with (13.4 ± 0.48) possibly due to its high surface charge and improved diffusion across the enzyme interface [43]. Whereas PLHN-G-D_2 had the lowest inhibition at (89.1 ± 0.27), due to its larger particle size and limited interaction with the lipoxygenase active site [45]. Regarding butyrylcholinesterase inhibition, notable compounds for butyrylcholinesterase inhibition are GCN-D_1, GCN-D_2, and PLHN-G-D_3, indicating that the interaction with cholinesterase active sites may be improved by gum-based carriers [46]. This analysis underscores the diverse efficacy of the compounds across various enzyme activities, highlighting key candidates with potential therapeutic applications. These findings align with previously reported studies showing that polymer–lipid hybrid nanoparticles offer superior encapsulation, controlled release, and enhanced biological response compared to polymeric nanoparticles alone [46].

Statistical Analysis

Across all biological assays, the nanoparticles showed clear and consistent differences in activity depending on their composition. For antioxidant activity, the ACN displayed a steady rise from ACN-D_1 to ACN-D_3 ($p < 0.0001$), while GCN followed the pattern GCN-D_3 < GCN-D_2 < GCN-D_1 ($p < 0.0005$). Within the PLHN-A, showed the highest activity in PLHN-A-D_2 ($p < 0.00001$), whereas in the PLHN-G activity increased from PLHN-G-D_1 to PLHN-G-D_3 ($p < 0.00001$ to $p \approx 0.005$). Anti-urease activity clearly varied with the type of nanoparticle. ACN-D_3 showed noticeably lower activity than ACN-D_1 and ACN-D_2 ($p < 0.00001$). All GCN differed significantly from one another ($p < 0.0001$). In the PLHN-A and PLHN-G, both showed meaningful differences across their individual types ($p < 0.009$ to $p < 0.00001$). Lipoxygenase inhibition also varied across the nanoparticle systems, with ACN and GCN showing progressive increases in activity ($p < 0.001$ and $p < 0.0005$, respectively). Within the PLHN-A, showed the highest activity in PLHN-A-D_2 ($p < 0.0001$), while the PLHN-G reached their strongest response in PLHN-G-D_2 ($p < 0.00001$). The IC_{50} values for butyrylcholinesterase inhibition further supported these trends. ACN potency increased steadily from ACN-D_1 to ACN-D_3 ($p < 0.0001$), GCN-D_3 showed significantly lower IC_{50} than GCN-D_1 and GCN-D_2 ($p < 0.001$), PLHN-A-D_2 was the most active among the PLHN-A ($p < 0.00001$), and both PLHN-G-D_1 and PLHN-G-$_2$ were more effective than PLHN-G-D_3 ($p < 0.0001$). Taken together, the results clearly indicate that differences between biopolymer-based nanoparticles and polymer-lipid-based nanoparticles have a strong impact on their biological activities across all assays.

Conclusion

This study demonstrates the therapeutic potential of isatin thiazole loaded nanoparticles based on their notable enzyme-inhibition and antioxidant activities. Two distinct nanoparticle systems, polysaccharide-based (ACN and GCN) and polymer-lipid hybrid nanoparticles (PLHN-A and PLHN-G) were systematically evaluated, and the results revealed that nanoparticle composition plays a crucial role in modulating biological activity. Among all tested nanoparticles, PLHN-A-D_3 exhibited the highest antioxidant activity, attributable to the synergistic interaction between sodium alginate and soya lecithin, that enhanced solubility, stability, and sustained drug release. ACN-D_3 showed significant antiurease activity, suggesting their potential in treating urease-

related infections such as those caused by *Helicobacter pylori*. Likewise, ACN-D_1 displayed strong lipoxygenase inhibition, highlighting their suitability for development of anti-inflammatory therapies. GCN-D_1 demonstrated effective butyrylcholinesterase inhibition, indicating their promise for neurological disorders such as Alzheimer's disease. Collectively, these findings underscore the critical role of biopolymer-based and hybrid nanoparticle system composition in enhancing biological activities. Future studies should prioritize in vivo validation, detailed pharmacokinetic profiling, and cytotoxicity assessment to establish clinical relevance.

References

1. Lu W., Shi Y., Wang R., Su D., Tang M., Liu Y., Li Z., Antioxidant activity and healthy benefits of natural pigments in fruits: a review, *Int. J. Mol. Sci.*, **22**, 4945 (2021).
2. A.M. Pisoschi, A. Pop, F. Iordache, L. Stanca , G. Predoi, A.I. Serban, Oxidative stress mitigation by antioxidants—an overview on their chemistry and influences on health status, *Eur. J. Med. Chem.*, **209**, 112891 (2021).
3. Y. Khan, M. Solangi, K.M. Khan, N. Ullah, J. Iqbal, Z. Hussain, I. A. Khan, U. Salar, M. Taha, Exploration of thiazine Schiff bases as promising urease inhibitors: design, synthesis, enzyme inhibition, kinetic analysis, ADME/T evaluation, and molecular docking studies, *Int. J. Biol. Macromol.*, **281**, 136361 (2024).
4. S. Ansari, Y. Yamaoka, Survival of *Helicobacter pylori* in gastric acidic territory, *Helicobacter*, **22**, 12386 (2017).
5. T. Ali Chohan, H. Saleem, A. Yaqub, R. Rafique, D.-E.-S. Malik, M. I. Tousif, U. Khurshid, Nutritional and medicinal plants as potential sources of enzyme inhibitors toward the bioactive functional foods: An updated review, *Crit. Rev. Food Sci. Nutr.*, **64**, 9805 (2024).
6. J.Z. Haeggstrom, C.D. Funk, Lipoxygenase and leukotriene pathways, Biochemistry, biology, and roles in disease, *Chem. Rev.*, **111**, 5866 (2011).
7. R. Dey, S. Dey, A. Samadder, A.K. Saxena, S. Nandi, Natural inhibitors against potential targets of cyclooxygenase, lipoxygenase and leukotrienes, *Comb. Chem. High Throughput Screen.*, **25**, 2341 (2022).
8. V. E. Steele, C. A. Holmes, E. T. Hawk, L. Kopelovich, R. A. Lubet, J. A. Crowell, C. C. Sigman, G. J. Kelloff, Lipoxygenase inhibitors as potential cancer chemopreventives, *Cancer Epidemiol. Biomarkers Prev.*, **8**, 467 (1999).
9. S. Basiouni, G. Tellez-Isaias, J. D. Latorre, B. D. Graham, V. M. Petrone-Garcia, H. R. El-Seedi, Anti-inflammatory and antioxidative phytogenic substances against secret killers in poultry, *Curr. Status Prospect. Vet. Sci.*, **10**, 55 (2023).
10. Z.R. Chen, J.B. Huang, S.L. Yang, F.F. Hong, Role of cholinergic signaling in Alzheimer's disease, *Molecules*, **27**, 1816 (2022).
11. A. Nordberg, C. Ballard, R. Bullock, T. Darreh-Shori, M. Somogyi, A review of butyrylcholinesterase as a therapeutic target in the treatment of Alzheimer's disease, *Prim. Care Companion CNS Disord.*, **15**, 26731 (2013).
12. A. Skrzypek, M. Karpińska, M. Juszczak, A. Grabarska, J. Wietrzyk, E. Krajewska-Kułak, Cholinesterases inhibition, anticancer and antioxidant activity of novel benzoxazole and naphthoxazole analogs, *Molecules*, **27**, 8511 (2022).
13. M. Bortolami, F. Pandolfi, V. Tudino, A. Messore, V. N. Madia, D. De Vita, New pyrimidine and pyridine derivatives as multitarget cholinesterase inhibitors: design, synthesis, and in vitro and in cellulo evaluation, *ACS Chem. Neurosci.*, **12**, 4090 (2021).
14. M. Bortolami, F. Pandolfi, V. Tudino, A. Messore, V. N. Madia, D. De Vita, Design, synthesis, and in vitro, in silico and in cellulo evaluation of new pyrimidine and pyridine amide and carbamate derivatives as multifunctional cholinesterase inhibitors, *Pharmaceuticals*, **15**, 673 (2022).
15. S.-H. Lee, B.-C. Kim, J.-K. Kim, H. S. Lee, M. Y. Shon, J. H. Park, Development of cholinesterase inhibitors using 1-benzyl piperidin-4-yl (α)-lipoic amide molecules, *Bull. Korean Chem. Soc.*, **35**, 1681 (2014).
16. V. Varun, S. Sonam, R. Kakkar, Isatin and its derivatives: a survey of recent syntheses, reactions, and applications, *Med. Chem. Commun.*, **10**, 351 (2019).
17. A. Andreani, S. Burnelli, M. Granaiola, A. Leoni, A. Locatelli, R. Morigi, Antitumor activity of 3-substituted isatin derivatives, *Eur. J. Med. Chem.*, **45**, 1374 (2010).
18. K. M. Khan, U. R. Mughal, A. Khan, F. Naz, S. Perveen, M. I. Choudhary, Synthesis and urease inhibitory activity of some novel 3-benzylidenechroman-4-ones, *Lett. Drug Des. Discov.*, **7**, 188 (2010).
19. I. Chiyanzu, C. Clarkson, P. J. Smith, J. Lehman, P. Rosenthal, K. Chibale, Synthesis and antiplasmodial activity of new 4-aminoquinoline derivatives, *Bioorg. Med. Chem.*, **13**, 3249 (2005).
20. T. A. Farghaly, A. M. A. Alnaja, H. A. El-Ghamry, M. R. Shaaban, Synthesis, characterization, molecular docking and anticancer evaluation of

novel thiazole-based heterocycles, *Bioorg. Chem.*, **102**, 104103 (2020).
21. B. Ali, K. M. Khan, U. Salar, S. Hussain, M. Ashraf, M. Riaz, Synthesis, molecular docking and urease inhibitory studies of new N-substituted isatin derivatives, *Bioorg. Chem.*, **79**, 363 (2018).
22. M. Ali, K. M. Khan, U. Salar, M. Ashraf, M. Taha, A. Wadood, Synthesis, molecular docking and kinetic studies of isatin derivatives as potent urease inhibitors, *Mol. Divers.*, **22**, 841 (2018).
23. F. Rahim, F. Malik, H. Ullah, A. Wadood, F. Khan, M. T. Javid, Synthesis, molecular docking and enzyme inhibitory studies of N-substituted isatin hydrazone derivatives as potential urease inhibitors, *Bioorg. Chem.*, **60**, 42 (2015).
24. M. Solangi, Kanwal, K. M. Khan, S. Chigurupati, F. Saleem, U. Qureshi, Isatin thiazoles as antidiabetic agents: synthesis, in vitro enzyme inhibitory activities, kinetics and in silico studies, *Arch. Pharm.*, **355**, 2100481 (2022).
25. W. H. De Jong, P. J. Borm, Drug delivery and nanoparticles: applications and hazards, *Int. J. Nanomed.*, **3**, 133 (2008).
26. A. Yusuf, A. R. Z. Almotairy, H. Henidi, O. Y. Alshehri, M. S. Aldughaim, Nanoparticles as drug delivery systems: a review of the implication of nanoparticles' physicochemical properties on responses in biological systems, Polymers, **15**, 1596 (2023).
27. C. Prakash, S. Raja, G. Saravanan, P. D. Kumar, T. P. Selvam, Synthesis and evaluation of antioxidant activities of some novel isatin derivatives and analogs, *Asian J. Res. Pharm. Sci.*, **1**, 140 (2011).
28. L. Dantas, A. Fonseca, J. Pereira, A. Furtado, P. Gomes, M. Fernandes-Pedrosa, A. Leite, M. Rêgo, M. Pitta, T. Lemos, Anti-inflammatory and antinociceptive effects of the isatin derivative (Z)-2-(5-chloro-2-oxoindolin-3-ylidene)-N-phenyl-hydrazinecarbothioamide in mice, *Braz. J. Med. Biol. Res.*, **53**, e10204 (2020).
29. M. N. Arshad, A. M. Asiri, Synthesis, molecular structure, quantum mechanical studies and urease inhibition assay of two new isatin-derived sulfonylhydrazides, *J. Mol. Struct.*, **1133**, 80 (2017).
30. A. M. Hussein, A. Al Bahir, Y. H. Zaki, O. M. Ahmed, A. F. Eweas, S. A. Elroby, M. A. Mohamed, Synthesis, in vitro antioxidant, anticancer activity and molecular docking of new thiazole derivatives, *Results Chem.*, **7**, 101508 (2024).
31. A. I. Shahin, S. Zaib, S.-O. Zaraei, R. A. Kedia, H. S. Anbar, M. T. Younas, T. H. Al-Tel, G. Khoder, M. I. El-Gamal, Design and synthesis of novel anti-urease imidazothiazole derivatives with promising antibacterial activity against *Helicobacter pylori*, *PLoS One*, **18**, e0286684 (2023).
32. J. Checa, J. M. Aran, Reactive oxygen species: drivers of physiological and pathological processes, *J. Inflamm. Res.*, **10**, 1057 (2020).
33. I. Gulcin, H. A. Alici, M. Cesur, Determination of in vitro antioxidant and radical scavenging activities of propofol, *Chem. Pharm. Bull.*, **53**, 281 (2005).
34. M. Biglar, K. Soltani, F. Nabati, R. Bazl, F. Mojab, M. Amanlou, A preliminary investigation of the jack-bean urease inhibition by randomly selected traditionally used herbal medicine, *Iran. J. Pharm. Res.*, **11**, 831 (2012).
35. A. Tappel, Lipoxidase, *Methods in Enzymol.*, Elsevier, New York, **5**, 539 (1962).
36. F. Rahim, H. Ullah, M. Taha, A. Wadood, M. T. Javed, W. Rehman, M. Nawaz, M. Ashraf, M. Ali, M. S. Sajid, Synthesis and in vitro acetylcholinesterase and butyrylcholinesterase inhibitory potential of hydrazide based Schiff bases, *Bioorg. Chem.*, **68**, 30 (2016).
37. A. Mukhopadhyay, L. Jacob, S. Venkataramani, Dehydro-oxazole, thiazole and imidazole radicals: insights into the electronic structure, stability and reactivity aspects, *Phys. Chem. Chem. Phys.*, **19**, 394 (2017).
38. A. W. Martinez, J. M. Caves, S. Ravi, W. Li, E. L. Chaikof, Effects of crosslinking on the mechanical properties, drug release and cytocompatibility of protein polymers, *Acta Biomater.*, **10**, 26 (2014).
39. W. Q. Cai, X. Liu, W. Chen, Z. Huang, C. Li, X. Huang, Q. Q. Yang, Synergistic effect of lecithin and alginate, CMC, or PVP in stabilizing curcumin and its potential mechanism, *Food Chem.*, **413**, 135634 (2023).
40. A. S. Gohari, L. Nateghi, L. Rashidi, S. Berenji, Preparation and characterization of sodium caseinate-apricot tree gum/gum Arabic nanocomplex for encapsulation of conjugated linoleic acid (CLA), *Int. J. Biol. Macromol.*, **261**, 129773 (2024).
41. C. He, Y. Hu, L. Yin, C. Tang, C. Yin, Effects of particle size and surface charge on cellular uptake and biodistribution of polymeric nanoparticles, *Biomaterials*, **31**, 3657 (2010).
42. L. Rhazi, L. Lakahal, O. Andrieux, N. Niamba, F. Depeint, D. Guillemet, Relationship between the molecular characteristics of Acacia gum and its functional properties, Food Chem., **328**, 126860 (2020).
43. C. Ding, Z. Li, A review of drug release mechanisms from nanocarrier systems, Mater. Sci. Eng. C, **76**, 1440 (2017).
44. B. E. Feller, J. T. Kellis Jr., L. G. Cascao-Pereira, C. R. Robertson, C. W. Frank, The role of

electrostatic interactions in protease surface diffusion and the consequence for interfacial biocatalysis, Langmuir, **26**, 18916 (2010).
45. X. Chen, Y. C. Wu, P. X. Gong, H. J. Li, Co-assembly of foxtail millet prolamin-lecithin/alginate sodium in citric acid–potassium phosphate buffer for delivery of quercetin, *Food Chem.*, **381**, 132268 (2022).
46. D. Sivadasan, M. H. Sultan, O. Madkhali, Y. Almoshari, N. Thangavel, Polymeric lipid hybrid nanoparticles (PLNs) as emerging drug delivery platform-A comprehensive review of their properties, preparation methods, and therapeutic applications, Pharmaceutics, **13**, 1291 (2021).
47. M. M. Rostamabadi, S. R. Falsafi, K. Nishinari, H. Rostamabadi, Seed gum-based delivery systems and their application in encapsulation of bioactive molecules, *Crit. Rev. Food Sci. Nutr.*, **63**, 9937 (2023).
48. A. Shilpa, S. S. Agrawal, A. R. Ray, Controlled delivery of drugs from alginate matrix, *J. Macromol. Sci., Part C: Polym. Rev.*, **43**, 187 (2003).